

# Fractal Scaling Models of Natural Oscillations in Chain Systems and the Mass Distribution of the Celestial Bodies in the Solar System

Hartmut Müller

Global Scaling Research Institute in memoriam Leonhard Euler, Munich, Germany. E-mail: info@globalscaling.de

The present paper interprets matter as a chain system of quantum harmonic oscillators. A fractal spectral model of resonant oscillations in chain systems of protons generates a scaling mass spectrum, that reproduces the mass distribution of the celestial bodies in the Solar System.

## 1 Introduction

Fractal scaling models [1] of natural oscillations in chain systems of harmonic oscillators are not based on any statements about the nature of the link or interaction between the elements of the oscillating chain system. Therefore the model statements are quite generally, what opens a wide field of possible applications.

In comparison with empty cosmic space, celestial bodies (stars, planets, moons, asteroids) are compressed matter and the contribution of nucleons to the bodies mass is about 99%. In the framework of the standard particle model, protons and neutrons are baryons, in which the proton connects to a lower quantum energy level and a much more stable state than the neutron. In addition, the proton and neutron have similar rest masses, what permits us to interpret protons and neutrons as similar quantum oscillators with regard to their rest masses.

Based on a fractal scaling model [1] of natural oscillations in this paper we will interpret matter as a chain system of many oscillating protons and find out spectral ranges where the oscillation process stability and energy efficiency are relative high or low.

## 2 Methods

On the base of continued fraction method [1] we will search the natural frequencies of a chain system of many vibrating protons on the lowest energy level (ground stage) in this form:

$$f = f_p \exp(S), \tag{1}$$

$f$  is a natural frequency of a chain system of vibrating protons,  $f_p$  is the natural oscillation frequency of one proton,  $S$  is a finite continued fraction with integer elements:

$$S = n_0 + \frac{1}{n_1 + \frac{1}{n_2 + \frac{1}{\ddots + \frac{1}{n_k}}}} = [n_0; n_1, n_2, \dots, n_k], \tag{2}$$

where  $n_0, n_1, n_2, \dots, n_k \in \mathbb{Z}$ . The continued fractions (2) are in the canonical form and have a discrete spectrum of eigenvalues. With the help of the Lagrange transformation [2] every continued fraction with integer partial denominators can

be represented as a continued fraction with natural partial denominators, that's always convergent. In this paper we will investigate spectra generated by convergent continued fractions (2). The present paper follows the Terskich [3] definition of a chain system, where the interaction between the elements proceeds only in their movement direction.

Model spectra (2) are not only logarithmic-invariant, but also fractal, because the discrete hyperbolic distribution of natural frequencies repeats itself on each spectral level  $k$ . We investigate continued fractions (2) with a finite quantity of layers  $k$ , which generate discrete spectra, because in this case all continued fractions  $S$  represent rational numbers. Therefore the free link  $n_0$  and the partial denominators  $n_1$  can be interpreted as "quantum numbers".

The partial denominators  $n_1$  run through positive and negative integer values. Maximum spectral density areas (spectral nodes) arise automatically on the distance of one logarithmic unit, where  $|n_1| \rightarrow \infty$ . Fig.1 shows the spectrum on the first layer  $k = 1$  for  $|n_1| = 2, 3, 4, \dots$  and  $|n_0| = 0, 1, 2, \dots$  (logarithmic representation). Integer  $S$ -values are labeled.



Fig. 1: The spectrum (2) on the first layer  $k = 1$ , for  $|n_1| = 2, 3, 4, \dots$  and  $|n_0| = 0, 1, 2, \dots$  (logarithmic representation). Integer  $S$ -values are labeled.

Ranges of relative low spectral density (spectral gaps) and ranges of relative high spectral density (spectral nodes) arise on each spectral layer. In addition to the first spectral layer, Fig. 2 shows the second spectral layer  $k = 2$  for  $|n_2| = 2, 3, 4, \dots$  and  $|n_1| = 2$  (logarithmic representation).

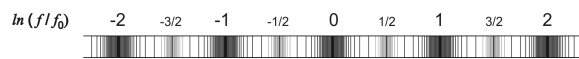


Fig. 2: The spectrum (2) on the first layer  $k = 1$ , for  $|n_0| = 0, 1, 2, \dots$  and  $|n_1| = 2, 3, 4, \dots$  and, in addition, the second layer  $k = 2$  for  $|n_1| = 2$  and  $|n_2| = 2, 3, 4, \dots$  (logarithmic representation).

In the spectral node ranges, where the spectral density reaches local maximum, natural frequencies are distributed maximum densely, so that near a spectral node almost each frequency is a natural frequency. The energy efficiency of

Celestial body	Body mass $m$ , kg	$\ln(m/m_p)$	$S$	$d$ , %
15 Eunomia (A)	$3.12 \times 10^{19}$ [8]	106.54	[106; 2]	0.037
Mimas (S)	$(3.7493 \pm 0.0031) \times 10^{19}$ [7]	106.73	[106; 2]	0.216
Miranda (U)	$(6.59 \pm 0.75) \times 10^{19}$ [8]	107.29	[107; 2]	-0.195
10 Hygiea (A)	$(8.98 \pm 0.01) \times 10^{19}$ [8]	107.60	[107; 2]	0.093
Enceladus (S)	$(1.08022 \pm 0.00101) \times 10^{20}$ [7]	107.78	[108]	-0.204
2 Pallas (A)	$(2.11 \pm 0.26) \times 10^{20}$ [8]	108.50	[108; 2]	0.001
4 Vesta (A)	$(2.67 \pm 0.02) \times 10^{20}$ [8]	108.69	[108; 2]	0.175
Tethys (S)	$(6.17449 \pm 0.00132) \times 10^{20}$ [7]	109.53	[109; 2]	0.028
1 Ceres (P)	$(9.43 \pm 0.07) \times 10^{20}$ [8, 9]	109.95	[110]	-0.045
Dione (S)	$(1.095452 \pm 0.000168) \times 10^{21}$ [7]	110.10	[110]	0.091
Umbriel (U)	$(1.172 \pm 0.135) \times 10^{21}$ [10]	110.10	[110]	0.091
Ariel (U)	$(1.350 \pm 0.120) \times 10^{21}$ [10]	110.23	[110]	0.209
Charon (P)	$(1.52 \pm 0.06) \times 10^{21}$ [11]	110.43	[110; 2]	-0.064
Iapetus (S)	$(1.805635 \pm 0.000375) \times 10^{21}$ [7]	110.60	[110; 2]	0.090
Rhea (S)	$(2.306518 \pm 0.000353) \times 10^{21}$ [7]	110.84	[111]	-0.144
Oberon (U)	$(3.014 \pm 0.075) \times 10^{21}$ [12]	111.12	[111]	0.108
Titania (U)	$(3.53 \pm 0.09) \times 10^{21}$ [12]	111.28	[111; 2]	-0.197
Haumea (P)	$(4.006 \pm 0.040) \times 10^{21}$ [13]	111.40	[111; 2]	-0.090
Pluto (P)	$(1.305 \pm 0.007) \times 10^{22}$ [11]	112.57	[112; 2]	0.018
Eris (P)	$(1.67 \pm 0.02) \times 10^{22}$ [14]	112.83	[113]	-0.150
Triton (N)	$2.14 \pm 10^{22}$ [15]	113.07	[113]	0.062
Europa (J)	$4.80 \pm 10^{22}$ [16]	113.88	[114]	-0.105
Moon (E)	$7.3477 \pm 10^{22}$	114.30	[114; 2]	-0.175
Io (J)	$(8.9319 \pm 0.0003) \times 10^{22}$ [16]	114.50	[114; 2]	0.001
Callisto (J)	$(1.075938 \pm 0.000137) \times 10^{23}$ [17]	114.69	[114; 2]	0.166
Titan (S)	$(1.3452 \pm 0.0002) \times 10^{23}$ [7]	114.91	[115]	-0.078
Ganymede (J)	$(1.4819 \pm 0.0002) \times 10^{23}$ [16]	115.00	[115]	0.001
Mercury	$(3.3022 \pm 0.0001) \times 10^{23}$	115.81	[116]	-0.164
Mars	$(6.4185 \pm 0.0001) \times 10^{23}$	116.47	[116; 2]	-0.026
Venus	$(4.8685 \pm 0.0001) \times 10^{24}$	118.50	[118; 2]	0.001
Earth	$(5.9722 \pm 0.0006) \times 10^{24}$ [18]	118.69	[118; 2]	0.160
Uranus	$(8.6810 \pm 0.0013) \times 10^{25}$ [12]	121.38	[121; 2]	-0.099
Neptune	$(1.0243 \pm 0.0015) \times 10^{26}$	121.55	[121; 2]	0.041
Saturn	$(5.6846 \pm 0.0001) \times 10^{26}$	123.27	[123; 2]	-0.186
Jupiter	$(1.8986 \pm 0.0001) \times 10^{27}$	124.47	[124; 2]	-0.024
Sun	$(1.9884 \pm 0.0002) \times 10^{30}$ [18]	131.42	[131; 2]	-0.061

Table 1: The masses of celestial bodies — planets, dwarf planets (P), asteroids (A), moons of Jupiter (J), Saturn (S), Uranus (U), Neptune (N) and Earth (E) and the  $S$ -values (6) of the nearest spectral nodes. The relative deviation  $d = (\ln(m/m_p) - S)/S$  is indicated in percents.

natural oscillations is very high. Therefore, if a frequency of an oscillation process is located near a node of the fractal spectrum (2), the process energy efficiency (degree of effectiveness) should be relative high. More detailed this topic is described in [1].

Let's assume that the oscillation amplitudes are low, the oscillations are harmonic and the energy level  $E_f$  of the vibrating protons depends only on their oscillation frequency ( $h$  is the Planck constant):

$$E_f = hf. \quad (3)$$

Atomic nuclei arise in the result of high energy processes of nucleosynthesis. Einstein's formula defines not only the connection between the rest energy and rest mass of nucleons, but also between binding energy and the mass defect of an atomic nucleus. Therefore we assume that the rest mass  $m$  of our model matter corresponds to the energy  $E_m$ :

$$E_m = mc^2. \quad (4)$$

Let's assume that the basis of nucleosynthesis is harmonic oscillations of protons and the energy (4) is identically

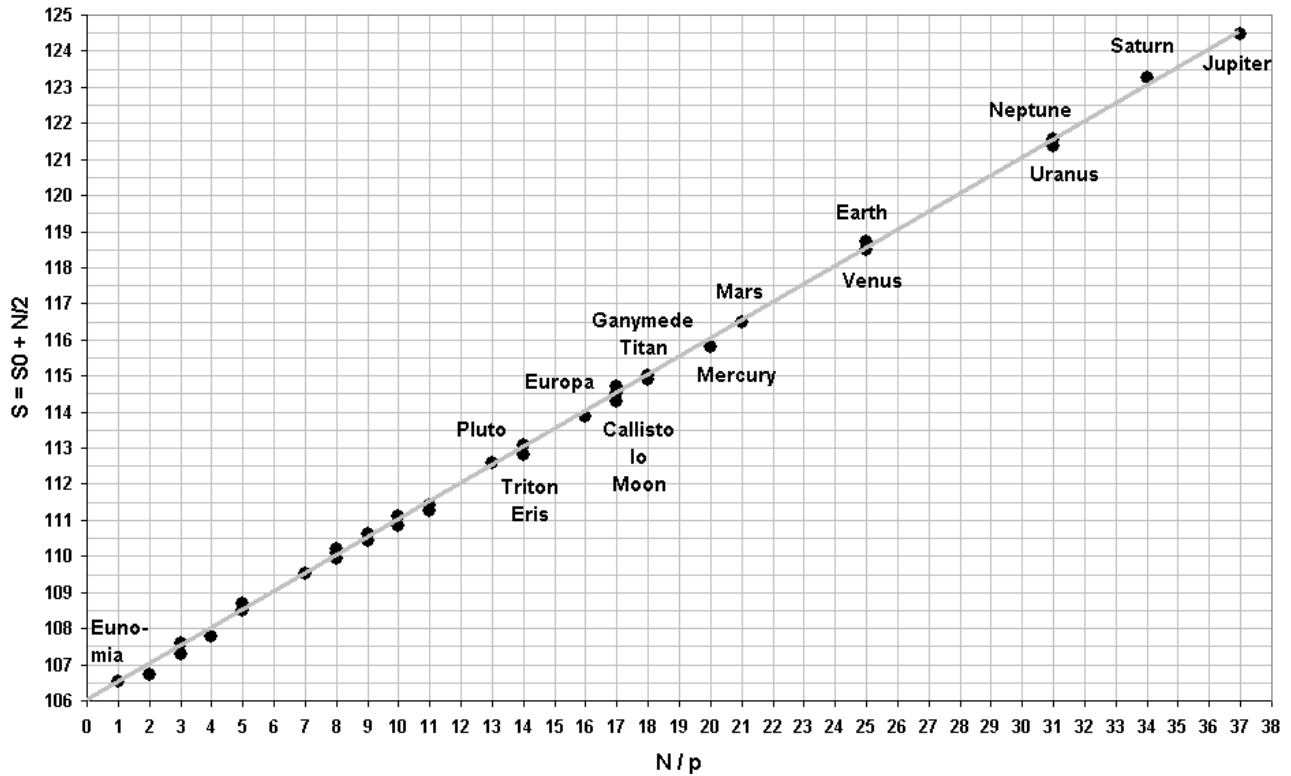


Fig. 3: The *S*-trajectory for  $S_0 = [106]$  and  $p = 1$ . Logarithmic scaling of Eunomia to Jupiter body mass.

with (3). In this case we can write:

$$m = f \frac{h}{c^2}. \tag{5}$$

In the framework of our oscillation model (1) the equation (5) means not only that mass can be changed into energy, but also that quantum oscillations generate the mass spectrum of our model matter. Under consideration of (1) now we can create a fractal scaling model of the natural mass spectrum of our model matter of vibrating protons. This mass spectrum is described by the same continued fraction (2), for  $m_p = f_p \frac{h}{c^2}$ :

$$\ln \frac{m}{m_p} = [n_0; n_1, n_2, \dots, n_k]. \tag{6}$$

Consequently, the frequency spectrum (2) and the mass spectrum (6) are isomorphic, and  $m_p$  is the proton rest mass  $1.672621637(83) \times 10^{-27}$  kg [4]. As mentioned already, we assume that mass generation processes are based on quantum natural oscillation processes. Celestial bodies are compressed matter, which consist of nucleons over 99%. Therefore we expect that the distribution of the celestial bodies in the proton resonance mass spectrum is not random and near spectral nodes the formation probability of massive bodies is maximum. Like in the Kundt's tube [5], near resonance nodes the matter accumulation reaches maximum intensity. The mass spectrum (6) is fractal and consequently it has a clear hierarchical structure, in which continued fractions (2) of the form  $[n_0]$  and  $[n_0; 2]$  define main spectral nodes, as Fig. 2 shows.

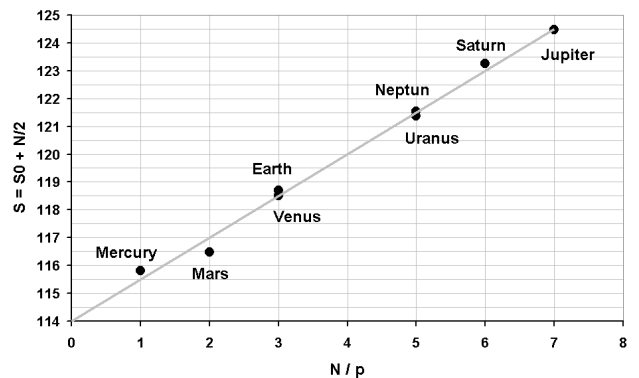


Fig. 4: The *S*-trajectory for  $S_0 = [114]$  and  $p = 3$ . Possibly, the extra-solar planet Gliese 581d could be a candidate of the node  $S = [120]$ .

### 3 Results

In the present paper we will compare the scaling mass spectrum (6) of our model matter in the range of  $10^{19}$  kg to  $10^{30}$  kg with the mass distribution of well-known celestial bodies. These are asteroids, planetoids, moons and planets of the Solar System (including the Sun), which masses were measured precisely enough and which are massive enough to be rounded by their own gravity.

For example, to locate the mass of the planet Venus in the scaling mass spectrum (6) of our model matter, one divides the Venus body mass by the proton rest mass and represents

Particle	Rest mass $m$ , MeV/c <sup>2</sup> [20]	$\ln(m/m_p)$	$S$	$d$ , %
electron	$0.510998910 \pm 0.000000013$	-7.515	[-7; -2]	-0.206
proton	$938.27203 \pm 0.00008$	0.000	[0]	0.000
W	$80398 \pm 25$	4,451	[4; 2]	1,089
Z	$91187.6 \pm 2.1$	4,577	[4; 2]	1,711

Table 2: The rest masses of the electron, proton and the W-Z-bosons and the  $S$ -values (6) of the nearest spectral nodes. The relative deviation  $d = (\ln(m/m_p) - S) / S$  is indicated in percent.

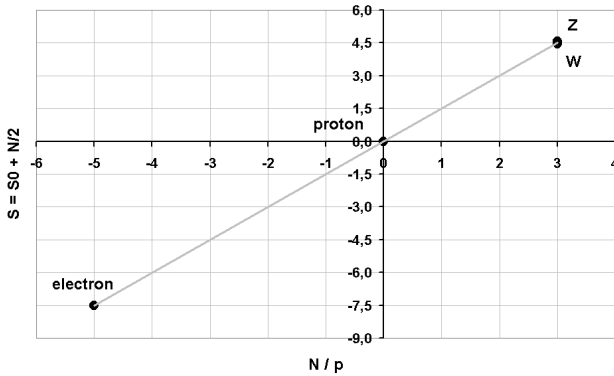


Fig. 5: The electron and W-Z-bosons rest masses lie on the  $S$ -trajectory for  $S_0 = [0]$  and  $p = 3$ . It's the same  $S$ -trajectory that shows Fig. 4, but prolonged down to negative  $N$ .

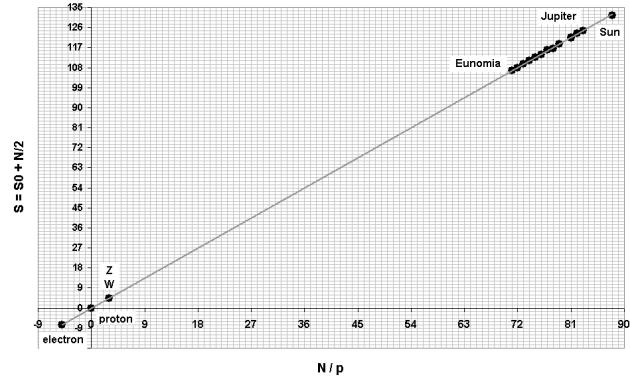


Fig. 6: The  $S$ -trajectory for  $S_0 = [0]$  and  $p = 3$ . Logarithmic scaling of the electron rest mass to the body mass of the Sun.

the logarithm as a continued fraction:

$$S_{venus} = \ln \frac{m_{venus}}{m_p} = \ln \left( \frac{4.869 \times 10^{24} \text{ kg}}{1.67262 \times 10^{-27} \text{ kg}} \right) \cong \cong 118.50 = 118 + \frac{1}{2}. \quad (7)$$

The analysis (6) of the Venus body mass takes the result  $n_0 = 118$ ,  $n_1 = 2$ . This means, that the Venus body mass corresponds to a spectral node on the first layer  $k = 1$  of the spectrum (6). The Sun mass is near the spectral node [131; 2]. It's also correct for the Alpha Centauri A and B masses. The Alpha Aquilae (Altair) mass is about 1.7 solar masses, that's near the node [132]. Table 1 shows the logarithms (6) calculated from the measured masses  $m$  of the celestial bodies and the  $S$ -values of the nearest spectral nodes.

Table 1 shows, that spectral nodes are occupied by bodies which have maximum mass in a local group or family. For example, the spectral node [115] is occupied by Ganymede and Titan, the most massive moons of Jupiter and Saturn, the spectral node [113] is occupied by Triton, the most massive moon of Neptune, the body mass of Eris, the largest defined dwarf planet, is also near the spectral node [113], but the spectral node [110] is occupied by Ceres, the most massive body of the asteroid belt. Mercury's mass is near the node [116]. Possibly, not Eris, but Mercury is the most massive dwarf planet in the Solar System. Actually, Mercury behaves like a dwarf planet, because it has the highest eccentricity of all the Solar System planets and it has the smallest axial tilt.

For the nodes  $[n_0]$  and  $[n_0; 2]$  the finite continued fraction (2) is  $S = n_0 + 1/n_1$  and the corresponding discrete mass values can be defined by linear  $S$ -trajectories, in which  $N \in \mathbb{Z}$ :

$$S = S_0 + \frac{N}{2}. \quad (8)$$

The prime divisibility of  $N = pn$ , in which  $p$  is a prime factor of  $N$ , defines sets of  $S$ -trajectories which form different sequences of mass-values  $m$  of the discrete spectrum (6).

$S$ -trajectories (8) present the discrete scaling mass distribution (6) very clear and can be interpreted as exponential equivalents to linear square-mass trajectories, which are a well-known systematic feature in the hadrons spectrum [6]. Fig. 3 shows the  $S$ -trajectory for  $S_0 = [106]$  and  $p = 1$ . Largest bodies are labeled. Possibly, vacant nodes are occupied by extrasolar bodies or bodies still to be discovered in the Solar System.

Possibly, the existence of the discrete spectrum (6) in the range of celestial bodies masses can be interpreted as "macroscopic quantization" [19]. The larger the bodies the more distinctive is this phenomenon. This can be recognized well at the example of the 8 largest planets in the Solar System, as Fig. 4 shows.

For  $S_0 = [0]$  and every  $p$  is  $m_0 = m_p$ , so that every  $S$ -trajectory can be prolonged down to the proton rest mass. Also the electron and W-Z-bosons rest masses lie on the  $S$ -trajectory for  $S_0 = [0]$  and  $p = 3$ , as Fig. 5 shows. Already within the eighties the scaling exponent  $3/2$  was found in the distribution of particle masses by Valery A. Kolombet [21].

Table 2 shows the logarithms (6) calculated from the measured particle rest masses, and the  $S$ -values of the nearest spectral nodes.

The  $S$ -trajectory in Fig. 5 is the same as the  $S$ -trajectory in Fig. 4, but prolonged down to the electron rest mass for  $S = [-7; -2]$ . Possibly, there is a fundamental link between particle rest masses and the masses of celestial bodies. Fig. 6 shows the  $S$ -trajectory for  $S_0 = [0]$  and  $p = 3$  in the range of  $-9 \leq S \leq 135$ , of the electron rest mass to the body mass of the Sun.

#### 4 Resume

In the framework of the present model discrete scaling distributions arise as result of natural oscillations in chain systems of harmonic oscillators. Particularly, the observable mass distribution of celestial bodies arise as result of natural oscillations in chain systems of protons, that can be understood as contribution to the fundamental link between quantum- and astrophysics. Possibly, the high energy efficiency of natural oscillations is the cause of the fractal scaling distribution of matter in the universe.

#### Acknowledgements

The author is deeply grateful to S. E. Shnoll, V. A. Panchevlyuga and V. A. Kolombet for valuable discussions and support.

Submitted on October 28, 2009 / Accepted on November 10, 2009

#### References

1. Muller H. Fractal scaling models of resonant oscillations in chain systems of harmonic oscillators. *Progress in Physics*, 2009.
2. Khintchine A. Ya. Continued fractions. University of Chicago Press, Chicago, 1964.
3. Terskich V. P. The continued fraction method. Leningrad, 1955 (*in Russian*).
4. Physical constants. Particle Data Group, [www.pdg.lbl.gov](http://www.pdg.lbl.gov)
5. Kundt A. Uber eine neue Art akustischer Staubfiguren und uber die Anwendung derselben zur Bestimmung der Schallgeschwindigkeit in festen Korpern und Gasen. *Annalen der Physik*, Leipzig, 1866, v. 127 (4), 497–523.
6. Forkel H., Beyer M., Frederico T. Linear square-mass trajectories of radially and orbitally excited hadrons in holographic QCD. arXiv: 0705.1857v2.
7. Jacobson R., Antreasian P., Bordi J. et al. The Gravity Field of the Saturnian System from Satellite Observations and Spacecraft Tracking Data. *Astronomical Journal*, 2006, v. 132, 2520–2526.
8. Baer J., Steven R. Astrometric masses of 21 asteroids, and an integrated asteroid ephemeris. *Celestial Mechanics and Dynamical Astronomy*. *Springer Science and Business Media*, 2008, v. 100, 27–42.
9. Carry B. et al. Near-Infrared Mapping and Physical Properties of the Dwarf-Planet Ceres. *Astronomy and Astrophysics*, 2007, v. 478, 235–244.
10. Uranus System Nomenclature Table Of Contents. Gazetteer of Planetary Nomenclature. USGS Astrogeology, 2009.
11. Marc W., William M, Eliot F et al. Orbits and photometry of Pluto's satellites: Charon, S/2005 P1, and S/2005 P2. *Astronomical Journal*, 2006, v. 132 (1), 290–298.
12. Jacobson R, Campbell J, Taylor A, Synnott S. The masses of Uranus and its major satellites from Voyager tracking data and Earth based Uranian satellite data. *Astronomical Journal*, 1992, v. 103 (6), 2068–2078.
13. Ragozzine D., Brown M. Orbits and Masses of the Satellites of the Dwarf Planet Haumea = 2003 EL61. *Astronomical Journal*, 2009. arXiv: 0903.4213v1.
14. Brown M, Schaller E. The Mass of Dwarf Planet Eris. *Science*, 2007, v. 316 (5831), 1585.
15. Neptune System Nomenclature Table Of Contents. Gazetteer of Planetary Nomenclature. USGS Astrogeology, 2009.
16. Showman A., Malhotra R. The Galilean Satellites. *Science*, 1999, v. 286, 77–84.
17. Anderson J., Jacobson R. et al. Shape, mean radius, gravity field and interior structure of Callisto. *Icarus*, v. 153, 157–161.
18. Astrophysical Constants and Parameters. Particle Data Group, [www.pdg.lbl.gov](http://www.pdg.lbl.gov)
19. Shnoll S. et al. Realization of discrete states during fluctuations in macroscopic processes, *Physics Uspekhi*, 1998, v. 41 (10), 1025–1035.
20. Particle listings. Particle Data Group, [www.pdg.lbl.gov](http://www.pdg.lbl.gov)
21. Kolombet V. Macroscopic fluctuations, masses of particles and discrete space-time, *Biofizika*, 1992, v. 36, 492–499 (*in Russian*).